

# Spatial and Temporal Distribution of Microplasma in Small Discharge Gaps

Marius Blajan

Member, IEEE  
Shizuoka University  
3-5-1 Johoku, Nakaku  
Hamamatsu, 432-8561, Japan  
blajanmarius@yahoo.com

Kazuo Shimizu

Member, IEEE  
Shizuoka University  
3-5-1 Johoku, Nakaku  
Hamamatsu, 432-8561, Japan  
shimizu@cjr.shizuoka.ac.jp

**Abstract** – Emission spectra were measured by use of an ICCD camera, and a spectrometer which was attached a fiber optic. Photos of microdischarges were taken using a microscope and a digital camera and an ICCD high speed camera. A self made fiber optic with 100  $\mu\text{m}$  diameter was used in order to have an accurate measurement of a small part of the microplasma discharge. A negative pulse Marx Generator was used to energize the electrodes. Experiments were carried out at atmospheric pressure in Ar and  $\text{N}_2/\text{Ar}$  mixture. Discharge voltage was negative pulse, rise time 100 ns, width 1  $\mu\text{s}$  at 1 kHz. The electrodes used had 3 mm holes diameter and the discharge gap was set at 100  $\mu\text{m}$ . Microplasma was measured in different points along the discharge gap. The spatial and temporal distribution showed characteristics that suggested the microplasma formation and its evolution across the discharge gap.

**Index Terms**—microplasma, dielectric barrier discharge, emission spectroscopy, pulse power, Marx Generator.

## I. INTRODUCTION

Microplasma applications are ranging from  $\text{NO}_x$  removal, indoor air treatment, to sterilization of bacteria or surface treatment of polymers [1-4]. Our microplasma is a dielectric barrier discharge at atmospheric pressure [5]. Among nonthermal plasma technologies, this technology has advantages due to its small size of reactor and power supply.

There are particularities of physics and fundamental aspects of microplasma that need to be studied in order to furthermore develop and optimize the applications. Emission spectroscopy and the imaging techniques methods for plasma analysis [6-11]. One of the characteristics of our microplasma is the small discharge gap below 100  $\mu\text{m}$  that makes difficult to measure and observe the phenomena. Dielectric barrier discharges have been used since Siemens proposed this technology for producing ozone. Eliasson et al. in their study [12] characterized the dielectric barrier discharges and the process of ozone synthesis from oxygen and reviewed also various techniques for the measurement and visualization of micro-discharges. We already reported some of the characteristics of microdischarges in microplasma [13]. In this paper a study regarding spatial and temporal distribution of microplasma is presented.

## II. EXPERIMENTAL SETUP

Emission spectra were measured by an ICCD camera

(Ryoushi-giken, SMCP-ICCD 1024 HAM-NDS/UV), and a spectrometer to which was attached a fiber optic (Fig. 1). Photos of microdischarges were taken using a high speed ICCD camera (Princeton Instruments, PI-MAX 3). A self made fiber optic with diameter of about 100  $\mu\text{m}$  was used in order to have an accurate measurement of a small part of the microplasma discharge. A negative pulse Marx Generator was used to energize the electrodes [7].

Emission spectroscopy experiments were carried out at atmospheric pressure in Ar and  $\text{N}_2/\text{Ar}$  mixtures. Discharge voltage was negative pulse, rise time 100 ns, width 1  $\mu\text{s}$  at 1 kHz (Fig. 2).

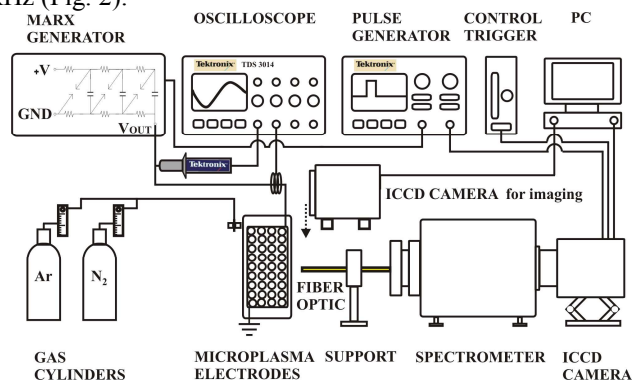


Fig. 1. Experimental setup

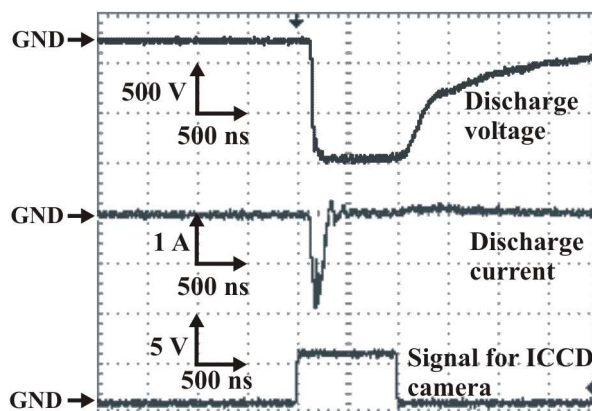


Fig. 2. Waveforms of discharge voltage, discharge current and gate signal for ICCD camera.

Due to small discharge gaps (0~100  $\mu\text{m}$ ) and to the assumed specific dielectric constant of the dielectric layer ( $\epsilon_r$

$= 10^4$ ), a high intensity electric field ( $10^7 \sim 10^8$  V/m) could be obtained with relatively low discharge voltages around 1 kV [1]. The electrode size was 20 mm versus 40 mm. They have holes to flow the gas, with a diameter of  $\varnothing$  3mm and an aperture ratio of 36%. The discharge gap was set at 100  $\mu$ m using a spacer. Microplasma was measured in different points along X axis by varying the position of the electrodes as shown in Fig. 3.

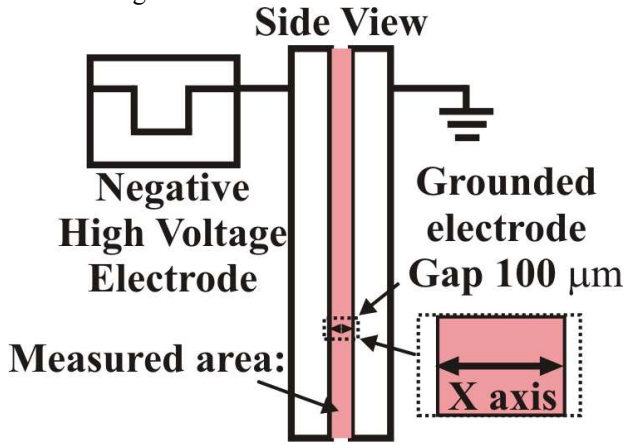


Fig. 3. Electrode arrangement for measuring spatial and temporal distribution of light emission.

### III. RESULTS AND DISCUSSIONS

#### A. Emission Spectroscopy

The emission spectrum of the microplasma discharge in Ar and Ar/N<sub>2</sub> mixture showed high intensity peaks of N<sub>2</sub> second positive band system (N<sub>2</sub> SPS 315.9 nm, 337.1 nm, 357.7 nm, 380.4 nm) [14] and OH peaks (306 ~ 309 nm) [15] (Fig. 4). The emission spectrum of the microplasma discharge in Ar in the ultraviolet region showed high intensity peaks of OH (Fig. 5).

For the discharge in pure Ar high intensity peaks corresponding to ArI were measured in the violet and red regions [16]. The highest Ar I intensity peak was measured at 696.5 nm (Fig. 6).

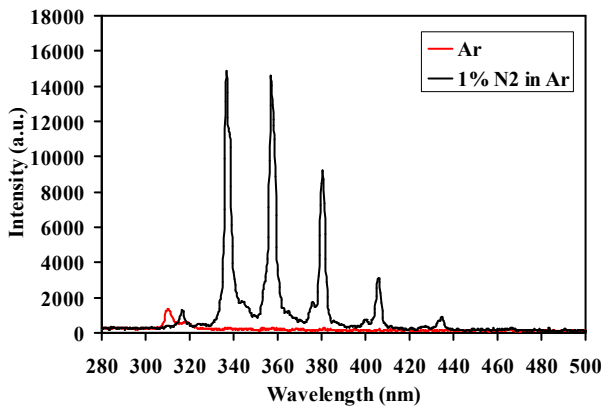


Fig. 4. Emission spectrum of microplasma in Ar and N<sub>2</sub>/Ar mixture in ultraviolet region. Discharge voltage was 1 kV.

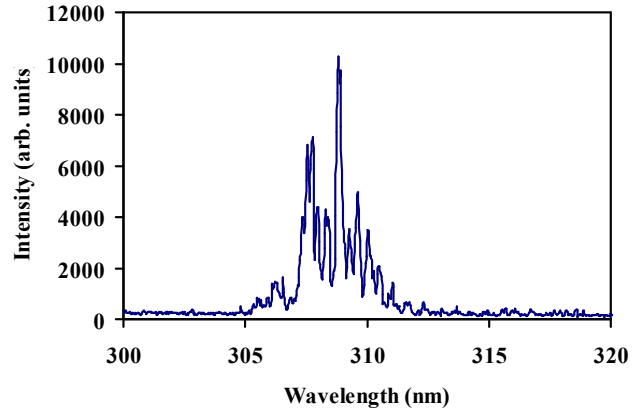


Fig. 5. OH peaks measured in microplasma discharge in Ar. Discharge voltage was 1 kV.

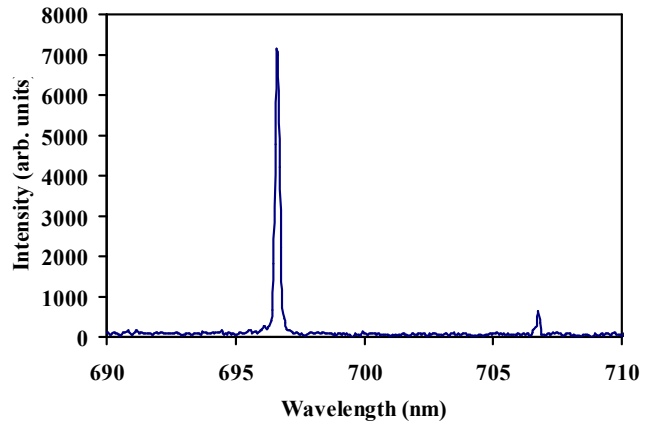


Fig. 6. Ar I peaks in red region for microplasma discharge in Ar. Discharge voltage was 1 kV.

#### B. Temporal Emission Measurements

The intensity of Ar I peak at 696.5 nm was measured along X axis using experimental setup shown in Fig. 3 by varying across X axis with 20  $\mu$ m incremental steps the position of electrodes versus the fiber optic. Microplasma was generated in pure Ar at 1 kV.

The gating of ICCD camera was temporally placed by varying the delay of the trigger circuit at moments corresponding to the time evolution of discharge current. It was considered the time origin the moment when discharge current started to rise. The opening time of ICCD camera was 15 ns with rise time and fall time of 6 ns each, thus it could be considered that the effective opening time was 3 ns.

The highest intensity was measured after 20 ns from the beginning of the discharge and the tendency is to evolve towards the cathode as shown in Fig. 7. The discharge gap was about 100  $\mu$ m as shown in the figure were with dotted lines are delimited the electrode walls. The delimitation of the electrodes and the position of the discharge gap on X axis could have some errors due to the asperities on the electrodes

which makes the discharge gap to vary with  $\pm 20\mu\text{m}$  from the stated  $100\ \mu\text{m}$ . The Ar I peak at  $696.5\ \text{nm}$  was the highest intensity peak of the emission in argon thus its time evolution could be correlated with discharge current characteristics.

Relative intensities corresponding to each incremental time step for the same peak are shown in Fig. 8. According to these values, it could be observed that at the initial moments of the discharge the intensity was higher towards the anode and after that it moved towards cathode.

The intensity of  $\text{N}_2$  SPS peak at  $337.1\ \text{nm}$  was measured along X axis. Microplasma was generated in  $1\% \text{N}_2$  in Ar at  $1\ \text{kV}$ .

Opening time of the camera was considered to be  $3\ \text{ns}$ . It was considered the time origin the moment when discharge current started to rise.

For each time step measurement along the X axis it was calculated the relative intensity of  $\text{N}_2$  SPS peak and plotted against the measurements positions on X axis (Fig. 9). The discharge gap was about  $100\ \mu\text{m}$  as shown in the figure were with dotted lines are delimited the electrode walls. The surface plot depicted in Fig. 9 represents only the relative intensities for each time step measurement. Thus measurement corresponding to one time the step could not be compared in term of absolute intensity with other but the plot shows how the area with highest intensity at a given moment varies inside the discharge gap. Thus it could be observed that at the beginning of discharge the highest intensity was measured near anode and after  $20\ \text{ns}$ , it started to shift towards cathode and back to anode after  $130\ \text{ns}$ .

The spatial and temporal distribution of intensity peak of  $\text{N}_2$  SPS at  $337.1\ \text{nm}$  could be interpreted as an indication of electron density [17-20].

The measurements of Ar I peak at  $696.5\ \text{nm}$  and OH peak at  $308.9\ \text{nm}$  were performed in a single point in the middle of the discharge gap at various time positions of discharge current.

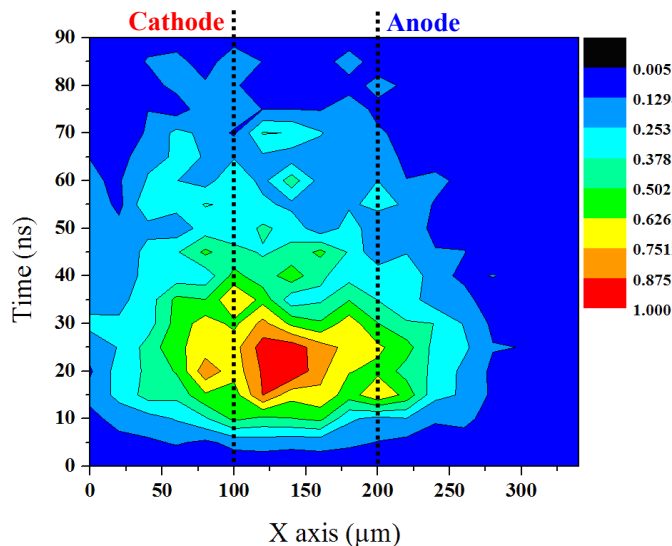


Fig. 7. Spatial distribution of Ar I intensities for microplasma discharge in Ar at  $1\ \text{kV}$ .

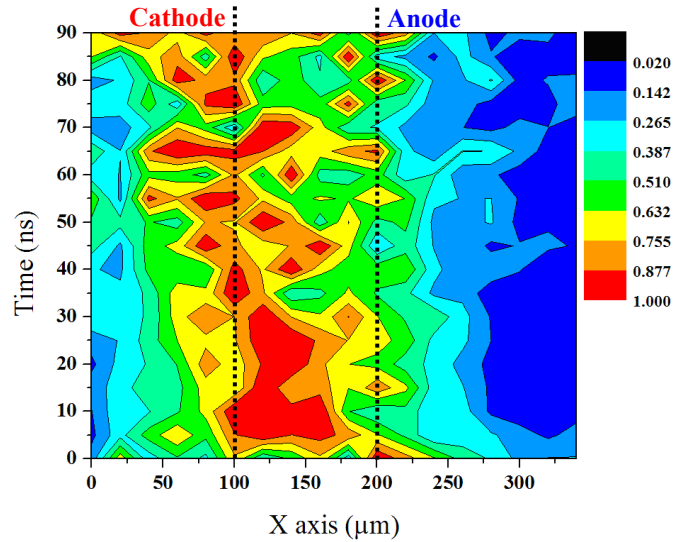


Fig. 8. Spatial distribution of Ar I relative intensities for microplasma discharge in Ar at  $1\ \text{kV}$ .

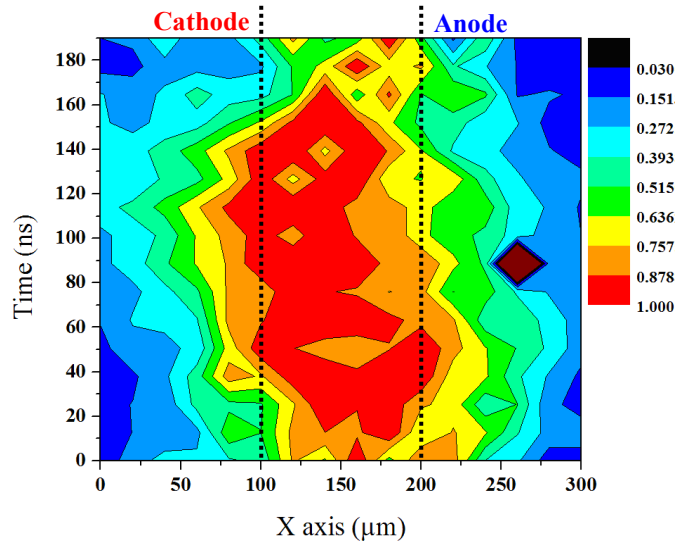


Fig. 9. Spatial distribution of  $\text{N}_2$  SPS peak at  $337.1\ \text{nm}$  relative intensities for microplasma discharge in  $1\% \text{N}_2$  in Ar at  $1\ \text{kV}$ .

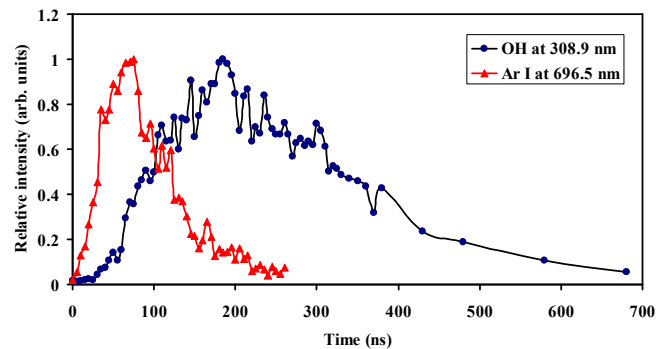


Fig. 10. Temporal evolution of Ar I peak at  $696.5\ \text{nm}$  and OH peak at  $308.9\ \text{nm}$  relative intensities during discharge.

The time increment was 5 ns. In Fig. 10 is shown that the temporal evolution of the intensities of Ar I peak which has the maximum intensity after about 75 ns and that of OH peak after about 185 ns. Moreover the maximum intensity of OH peak corresponds to the almost lowest value of emission for the Ar I peak. This suggests that the OH radical was generated not by direct electron impact but by the reaction with excited Ar. The time origin was considered the beginning of the discharge current rise. The OH peak intensities were measured up to 680 ns when the value of the discharge current was almost 0.

Thus the presence of emission corresponding to OH peak could be attributed to the interaction of the metastable Ar atom with the traces of the water vapor in the reactor [21]. Metastables Ar\* ( $^3P_2$ ) can dissociate or excite H<sub>2</sub>O molecules to OH ( $A^2\Sigma$ ) [22]:



### C. Observation of Microdischarge

Dynamics of microdischarge was observed with high speed ICCD camera for microplasma in 1% N<sub>2</sub> in Ar at 1 kV. Gate time of ICCD camera was set at 3 ns (Fig. 11). The trigger signal was set initially at the time when the discharge current started to rise and this was considered as time origin. The time setting was then increased with 5 ns for each measurement.

Images show that with each 5 ns incremental steps the distribution of light emission in the gap was different suggesting the waves of light intensity that started directly from the anode (grounded) and propagate towards the negative one (cathode) (Fig. 12). The initial electron avalanche starting from cathode until reaches the anode and after the cathode directed streamer could be considered that was captured in the first image from Fig. 12. The gating of ICCD camera was set at 3 ns thus first image shows the phenomena up to 3 ns. Then the cathode layer development and cathode layer enhancement were observed [23-24].

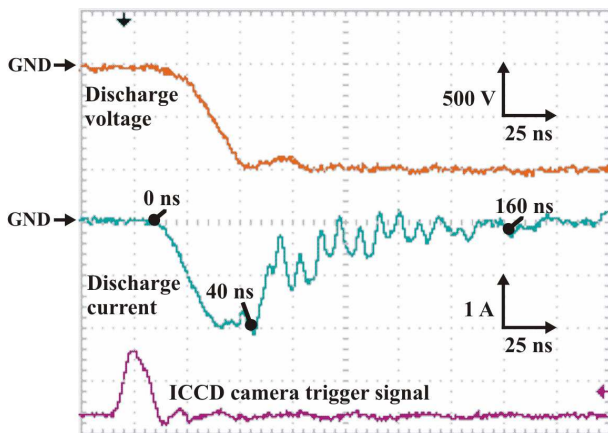


Fig. 11. Discharge voltage, corresponding discharge current and gate signal for ICCD camera for the microplasma discharge in 1% N<sub>2</sub> in Ar.

The initial phenomena of electron avalanche from cathode and the cathode directed streamer are difficult to capture mainly due to the small discharge gap characteristic to our microplasma. Finally the post discharge phenomena was observed starting from about 110 ns. Weak light intensity was measured up to 265 ns. According to N. Sewraj *et al.* the electron avalanche from cathode has an average speed of  $2.5 \times 10^5$  m/s and the cathode directed streamer an average speed of  $5 \times 10^5$  m/s [23]. This data was obtained at 50 torr in pure nitrogen. Thus in a 100  $\mu\text{m}$  discharge gap considering the above mention speeds the electron avalanche from cathode needs 0.4 ns to reach the anode and after the cathode directed streamer reaches the cathode in 0.2 ns.

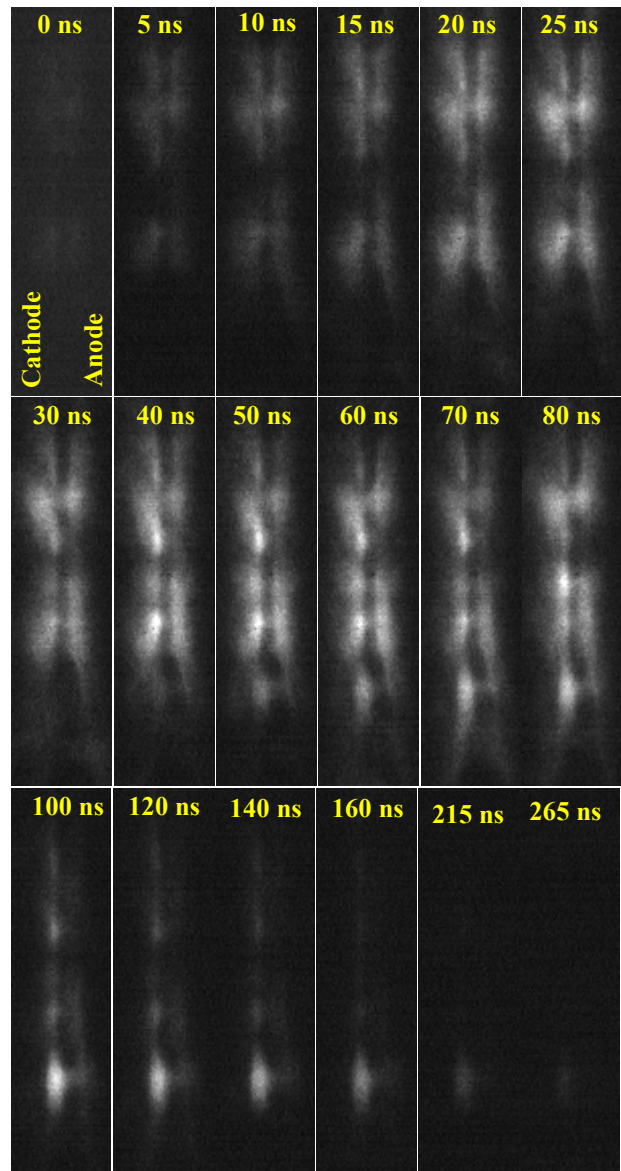


Fig. 12. Temporal evolution of light intensity during microplasma discharge in 1% N<sub>2</sub> in Ar at 1 kV.

The evolution of the optical emission was recorded at atmospheric pressure for a DBD in He at atmospheric by F. Iza et al [25]. Phenomena recorded for plasma generated with a 250 ns pulse in a 3 mm gap showed how emission started from anode and moved to cathode within a time period of about 40 ns then up to 110 ns the mission became more intense across the gap.

#### IV. CONCLUSION

Emission spectroscopy and imaging measurements were carried out for analyzing the spatial and temporal evolution of microplasma. The following conclusions were obtained:

1) Spatial and temporal distribution for the Ar I peak at 696.54 nm and N<sub>2</sub> SPS peak at 337.1 nm inside the discharge gap shown a maximum intensity towards the anode for the 20 ns corresponding to the rise time of discharge current and it shifted after towards cathode.

2) Spatial and temporal distribution of light emission from microplasma in 1% N<sub>2</sub> in Ar was observed for about 265 ns corresponding to the duration of discharge current. Light near the negative electrode was preceded by the waves of light intensity that started directly from the anode and propagated towards the cathode.

This clarifies some of the fundamental aspects of microplasma which can lead to a furthermore development and optimization of the technology for various applications.

#### ACKNOWLEDGMENT

The authors are thankful to Prof. Masaaki Nagatsu and Prof. Akihisa Ogino from Shizuoka University for the fruitful discussions.

#### REFERENCES

- [1] K. Shimizu, M. Yamada, M. Kanamori, M. Blajan, "Basic Study of Bacteria Inactivation at Low Discharge Voltage by Using Microplasmas," *IEEE Trans. Ind. Appl.*, Vol. 46, No. 2, pp. 641- 649, 2010.
- [2] M. Blajan, A. Umeda, S. Muramatsu, and K. Shimizu, "Emission Spectroscopy of Pulsed Powered Microplasma for Surface Treatment of PEN Film," *IEEE Trans. Ind. Appl.*, Vol. 47, pp. 1100-1108, 2011.
- [3] K. Shimizu, M. Blajan, and T. Kuwabara, "Removal of Indoor Air Contaminant by Atmospheric Microplasma," *IEEE Trans. Ind. Appl.*, Vol. 47, pp. 2351-2358, 2011.
- [4] K. Shimizu, A. Umeda, M. Blajan, "Surface Treatment of Polymer Film by Atmospheric Pulsed Microplasma: Study on Gas Humidity Effect for Improving the Hydrophilic Property," *Jpn. J. Appl. Phys.*, Vol. 50, 08KA03, 2011.
- [5] K. Shimizu, A. Umeda, S. Muramatsu, M. Blajan, "Basic Study on Surface Treatment of Functional Resin Film by Pulsed Atmospheric Microplasma," *IEEJ Transaction on Fundamentals and Materials*, Vol. 130, 858-864, 2010.
- [6] F. Iza, G. J. Kim, S. M. Lee, J. K. Lee, J. M. Walsh, Y. T. Zhang, M. G. Kong, "Microplasmas: sources, particle kinetics, and biomedical applications," *Plasma Process. Polym.*, vol. 5, pp. 322-344, 2008.
- [7] K. Shimizu, T. Ishii, M. Blajan, "Emission Spectroscopy of Pulsed Power Microplasma for Atmospheric Pollution Control," *IEEE Trans. Ind. Appl.*, Vol. 46, No. 3, pp. 1125-1131, 2010.
- [8] J. Machala, M. Janda, K. Hensel, I. Jedlovsky, L. Lestinska, V. Foltin, V. Martisovits, M. Morvova, "Emission spectroscopy of atmospheric pressure plasmas for bio-medical and environmental applications," *J. Mol. Spectrosc.*, vol. 243, pp. 194-201, 2007.
- [9] N. Srivastava and C. Wang, "Determination of OH Radicals in an Atmospheric Pressure Helium Microwave Plasma Jet," *IEEE Trans. Plasma Sci.*, Vol. 39, pp. 918-924, 2011.
- [10] Z. Kregar, N. Krstulovic, S. Milosevic, K. Kenda, U. Cvelbar, and M. Mozeti, "Inductively Coupled RF Oxygen Plasma Studied by Spatially Resolved Optical Emission Spectroscopy," *IEEE Trans. Plasma Sci.*, Vol. 36, pp. 1368-1369, 2008.
- [11] Z. Kregar, M. Biscan, S. Milosevic, and A. Vesel, "Monitoring Oxygen Plasma Treatment of Polypropylene With Optical Emission Spectroscopy," *IEEE Trans. Plasma Sci.*, Vol. 39, pp. 1239-1246, 2011.
- [12] B. Eliasson, M. Hirth, and U. Kogelschatz, "Ozone synthesis from oxygen in dielectric barrier discharges," *J. Phys. D, Appl. Phys.*, vol. 20, pp. 1421-1437, 1987.
- [13] M. Blajan, and K. Shimizu, "Phenomena of Microdischarges in Microplasma," *IEEE Trans. Plasma Sci.*, Digital Object Identifier 10.1109/TPS.2012.2190994.
- [14] A. Lofthus, P. H. Krupenie, "The spectrum of molecular nitrogen," *J. Phys. Chem. Ref. Data*, vol. 6, no. 1, pp. 113-307, 1977.
- [15] F. Liu, W. Wang, S. Wang, W. Zheng, and Y. Wang, "Diagnosis of OH radical by optical emission spectroscopy in a wire-plate bi-directional pulsed corona discharge," *J. Electrostat.*, Vol. 65, pp. 445-451, 2007.
- [16] Göran Norlén, "Wavelengths and Energy Levels of Ar I and Ar II based on New Interferometric Measurements in the Region 3400-9800 Å," *Physica Scripta*, vol. 8, pp. 249-268, 1973.
- [17] T. Hoder, M. Sira, K. V. Kozlov, and H. E. Wagner, "Investigation of the coplanar barrier discharge in synthetic air at atmospheric pressure by cross-correlation spectroscopy," *J. Phys. D: Appl. Phys.*, Vol. 41, 035212, 2008.
- [18] K. V. Kozlov and H.-E. Wagner, "Progress in spectroscopic diagnostics of barrier discharges," *Contrib. Plasma Phys.*, vol. 47, no. 1/2, pp. 26-33, Feb. 2007.
- [19] K. V. Kozlov, H.-E. Wagner, R. Brandenburg, and P. Michel, "Spatiotemporally resolved spectroscopic diagnostics of the barrier discharge in air at atmospheric pressure," *J. Phys. D, Appl. Phys.*, vol. 34, no. 21, pp. 3164-3176, Nov. 2001.
- [20] H.-E. Wagner, R. Brandenburg, K.V. Kozlov, A. Sonnenfeld, P. Michel, J.F. Behnke, "The barrier discharge: basic properties and applications to surface treatment," *Vacuum*, Vol. 71, pp. 417-436, 2003.
- [21] I. Vinogradov, D. Zimmer, A. Lunk, "Diagnostics of SiCOH-Film-Deposition in the Dielectric Barrier Discharge at Atmospheric Pressure," *Plasma Process. Polym.*, Vol. 4, pp. S435-S439, 2007.
- [22] D. Nie, W. Wang, D. Yang, H. Shi, Y. Huo, L. Dai, "Optical study of diffuse bi-directional nanosecond pulsed dielectric barrier discharge in nitrogen," *Spectrochimica Acta Part A*, vol. 79, pp. 1896-1903, 2011.
- [23] N. Sewraj, R. J. Carman, N. Merbahi, F. Marchal, and E. Leysenne, "Spatiotemporal Distribution of a Monofilamentary Dielectric Barrier Discharge in Pure Nitrogen," *IEEE Trans. Plasma Sci.*, Vol. 39, pp. 2128-2129, 2011.
- [24] R. Ono and T. Oda, "Formation and structure of primary and secondary streamers in positive pulsed corona discharge—effect of oxygen concentration and applied voltage," *J. Phys. D: Appl. Phys.*, Vol. 36, pp. 1952-1958, 2003.
- [25] F. Iza, J. L. Walsh, and M. G. Kong, "From Submicrosecond- to Nanosecond-Pulsed Atmospheric-Pressure Plasmas," *IEEE Trans. Plasma Sci.*, Vol. 37, pp. 1289-1296, 2009.